

Investigating an imaging condition for nonlinear imaging – principles and application to reverse-time-migration artifacts removal

Clement Fleury*, Center for Wave Phenomena, Colorado School of Mines, and Ivan Vasconcelos, ION Geophysical, GXT Imaging Solutions

SUMMARY

Imaging highly complex structures is a challenging problem in seismic imaging because it can involve dealing with nonlinear scattering effects (e.g., migration of multiples, amplitude corrections for transmission effects). In this context, two-way wave-equation methods have received increasing interest because they allow for the migration of multiply scattered events at their correct locations in the subsurface. The classic imaging condition consists of the zero-lag crosscorrelation of the downgoing source wavefield with the upgoing receiver wavefield. By nature, this imaging condition relies on a single-scattering approximation, and thus cannot account properly for multiply scattered waves. To express an imaging condition suitable for nonlinear problems, we modify the imaging condition using scattering representations. This new imaging condition builds on previously established connections between seismic imaging and scattering-based image-domain interferometry. Our method consists of modifying the conventional imaging condition to account for the autocorrelation of scattered waves in the receiver wavefields. We address the principles of our nonlinear imaging conditions, and discuss its importance in ideal nonlinear imaging experiments. In practice, however, the nonlinear imaging approach we present faces unsolved challenges regarding limitations in survey design (e.g., limited source and receiver aperture) as well as limitations in current back-propagation approaches. One immediate potential application of our technique lies in adaptive removal of the model-induced artifacts commonly encountered in reverse-time migration (RTM). To remove RTM artifacts, we use our nonlinear imaging condition in an adaptive filtering scheme based on regularized non-stationary regression. We illustrate these concepts with numerical examples using the Sigsbee model.

INTRODUCTION

Two-way wave-equation imaging techniques, including reverse-time-migration (Baysal et al., 1983; McMechan, 2006) and full waveform inversion (Tarantola, 1984; Pratt, 1999) are designed to account, in principle, for nonlinear effects in imaging of finite-frequency data in the presence of complex subsurface models. Most of these imaging methods, however, rely on the classic imaging condition that fundamentally requires a single-scattering approximation. The downgoing source wavefield is crosscorrelated with the upgoing receiver wavefield to get an estimate of the reflection coefficient at zero time-lag (Claerbout, 1971).

Recently, this imaging condition has been extended to non-zero time and space lags (Rickett and Sava, 2002; Sava and Fomel, 2006). Using representation theorem for scattered waves,

Sava and Vasconcelos (2010) have interpreted the resulting extended images as evaluations of locally scattered wavefields in the image domain. We expand this interpretation to define a new imaging condition that accounts for multiply scattered waves. Crosscorrelating multiply scattered waves gives rise to erroneous events which the classic imaging condition maps in the image space. In seismic interferometry, these spurious arrivals are reduced by crosscorrelating scattered waves with themselves (Snieder et al., 2008; Fleury et al., 2010). By analogy, we hypothesize that the addition of the autocorrelation of scattered waves present in the receiver wavefields generated in wave-equation imaging can attenuate imaging artifacts.

In seismic imaging, the receiver wavefield, however, is an extrapolation of scattered waves (Esmersoy and Oristaglio, 1988), and the back-extrapolation of the receiver wavefield is hindered by limited source and receiver apertures as well as errors in the models used for wavefield extrapolation (Vasconcelos et al., 2010). Furthermore, using only pressure data in acoustic back-propagation (i.e., in the absence of particle velocity sources and receivers) leads to additional amplitude errors in wavefield extrapolation. When combined, these limitations of receiver wavefield extrapolation generate the need for the autocorrelation of the receiver wavefield to be adaptively summed to the conventional correlation of source and receiver wavefields in our proposed imaging condition. The image obtained by autocorrelation of receiver wavefield is adaptively added to the one obtained with the classic imaging condition. We use a non-stationary matching filtering method (Fomel, 2009) to carry out this adaptive summation.

First, we present our nonlinear imaging condition, discussing its role in ideal imaging experiments. Then, we analyze the behavior of our method in reverse-time migration using a numerical experiment, where we elaborate on the necessity of the adaptive filtering scheme and illustrate its potential for RTM artifact removal.

IMAGING CONDITION FOR NONLINEAR IMAGING

Theory

The analogy between imaging and interferometry (Vasconcelos et al., 2010) has been used to define the image I as

$$I(\mathbf{x}) = G_S(\mathbf{x}, \mathbf{x}, \tau = 0) = \int G_S(\mathbf{x}, \mathbf{x}, \omega) d\omega ; \quad (1)$$

that is, a representation of the locally scattered wavefield G_S between two points coinciding in space at the image point \mathbf{x} , and evaluated at time $\tau = 0$. The representation theorem of the correlation-type for scattered acoustic waves (Vasconcelos

Adaptive imaging condition for nonlinear imaging

et al., 2009) is in the frequency domain (ω) given by

$$\begin{aligned} G_S(\mathbf{x}, \mathbf{x}, \omega) &= 2 \oint_{\delta\mathbb{D}} G_0^*(\mathbf{x}, \mathbf{r}, \omega) G_S(\mathbf{x}, \mathbf{r}, \omega) d^2r \\ &+ \frac{1}{j\omega} \int_{\mathbb{D}} V(\mathbf{r}, \omega) |G_0(\mathbf{x}, \mathbf{r}, \omega)|^2 d^3r \quad (2) \\ &+ \frac{1}{j\omega} \int_{\mathbb{D}} V(\mathbf{r}, \omega) G_0^*(\mathbf{x}, \mathbf{r}, \omega) G_S(\mathbf{x}, \mathbf{r}, \omega) d^3r, \end{aligned}$$

where \mathbb{D} is the imaging domain bounded by $\delta\mathbb{D}$, V is the scattering potential, and G_0 is the wavefield that propagates in the reference model (e.g., migration velocity model). Therefore,

$$\begin{aligned} I(\mathbf{x}) &= 2 \oint_{\delta\mathbb{D}} \left(\int G_0^*(\mathbf{x}, \mathbf{r}, \omega) G_S(\mathbf{x}, \mathbf{r}, \omega) d\omega \right) d^2r \quad (3) \\ &+ \int_{\mathbb{D}} \left(\int \frac{1}{j\omega} V(\mathbf{r}, \omega) G_0^*(\mathbf{x}, \mathbf{r}, \omega) G_S(\mathbf{x}, \mathbf{r}, \omega) d\omega \right) d^3r. \end{aligned}$$

Expression (3) defines an imaging condition (IC), generalizing the classic imaging condition (Claerbout, 1971, 1985). The classic image I_1 is obtained by crosscorrelating the source wavefield (modeling of G_0) and the receiver wavefield (extrapolation of G_S), and summing over sources located on $\delta\mathbb{D}$:

$$I_1(\mathbf{x}) = \oint_{\delta\mathbb{D}} \left(\int G_0^*(\mathbf{x}, \mathbf{r}, \omega) G_S(\mathbf{x}, \mathbf{r}, \omega) d\omega \right) d^2r. \quad (4)$$

In the classic image, the volume integral on the right-hand side of (3), which contains the nonlinearity with respect to the scattering potential, is neglected. This makes the classic IC unsuitable for nonlinear imaging, which does require the evaluation of the volume term in equation (3) (Vasconcelos et al., 2010).

Although in principle the evaluation of the volume term in equation (3) should account for nonlinear effects, this evaluation is computationally challenging because it requires modeling sources at every point inside the volume (Vasconcelos et al., 2010). The nonlinear IC we present here is designed to precisely circumvent the computation of the volume term, without any loss of generality. As an alternative to equation (4), we modify the imaging condition according to a representation theorem for the real part of the scattered field G_S ,

$$\begin{aligned} \Re[G_S(\mathbf{x}, \mathbf{x}, \omega)] &= 2 \oint_{\delta\mathbb{D}} \Re[G_0^*(\mathbf{r}, \mathbf{x}, \omega) G_S(\mathbf{r}, \mathbf{x}, \omega)] d^2r \\ &+ \oint_{\delta\mathbb{D}} |G_S(\mathbf{r}, \mathbf{x}, \omega)|^2 d^2r, \quad (5) \end{aligned}$$

where now the volume terms are replaced by the surface integral of the power of the scattered wavefield $|G_S(\mathbf{r}, \mathbf{x}, \omega)|^2$ (Carney et al., 2004). Since the image defined in (1) can be obtained via

$$I(\mathbf{x}) = \int \Re[G_S(\mathbf{x}, \mathbf{x}, \omega)] d\omega, \quad (6)$$

the new image I_2 is defined as

$$I_2(\mathbf{x}) = I_1(\mathbf{x}) + I_S(\mathbf{x}), \quad (7)$$

where

$$I_S(\mathbf{x}) = \frac{1}{2} \oint_{\delta\mathbb{D}} \left(\int |G_S(\mathbf{r}, \mathbf{x}, \omega)|^2 d\omega \right) d^2r. \quad (8)$$

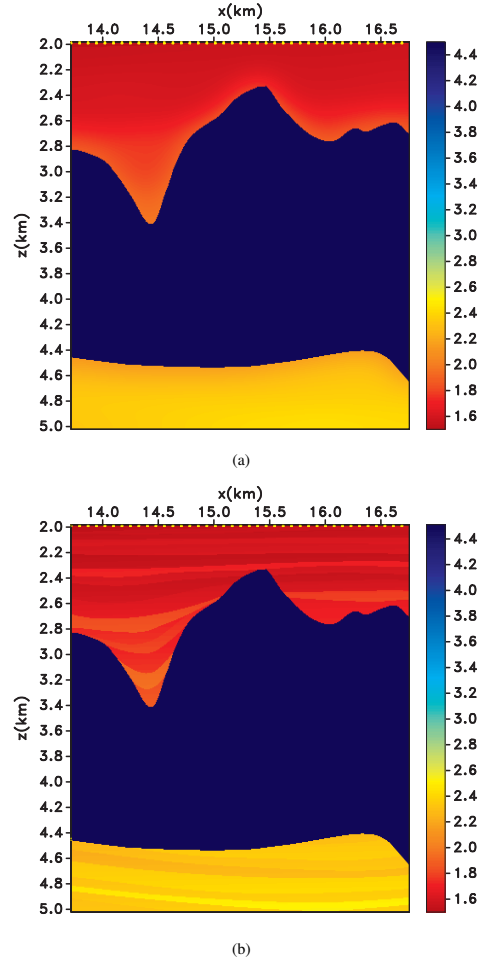


Figure 1: (a) is the background velocity model and (b) is the stratigraphic velocity model used in the synthetic examples.

Ideally, the image I_S obtained by autocorrelation of the receiver wavefield compensates for the nonlinear effects neglected in definition (4). Physically, the addition of the extra term in equation (8) follows from energy conservation: it corresponds to the power loss associated with the scattered field (Carney et al., 2004). This term, albeit being zero-phase, can have non-negligible side lobes in presence of multiple scattering that must be accounted for in the imaging condition.

Example

Imaging conditions (4) and (7) are compared for the synthetic model presented in Figure 1 (subset of Sigsbee 2A model). The background model (Figure 1(a)) is used to model G_0 . The stratigraphic model (Figure 1(b)) allows for the computation of the exact scattered wavefield G_S . An array of sources is located at 2 km depth. This example is referred as “case study”. The classic image I_1 (Figure 2) contains strong artifacts due to the presence of multiply scattered waves resulting from the high velocity contrast at the interface with the salt. After addition of image I_S (Figure 3), the new image I_2 reveals the structure of the image in its top salt portion without altering reflectors in the subsalt (Figure 4).

Adaptive imaging condition for nonlinear imaging

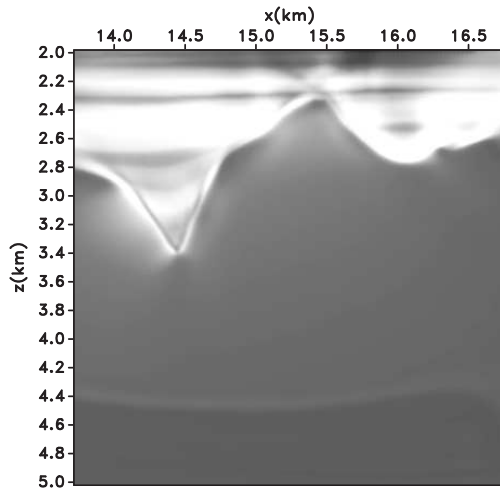


Figure 2: Classic image I_1 in the “case study”

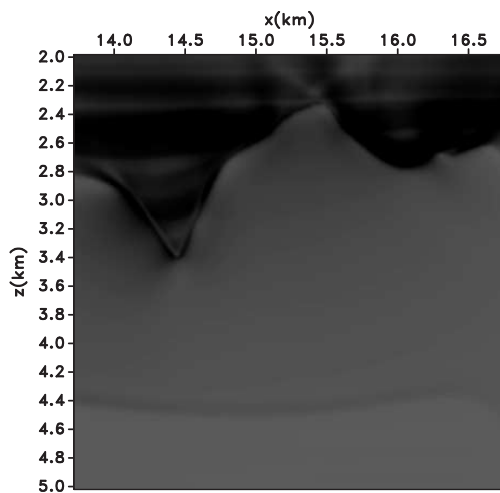


Figure 3: Image I_5 in the “case study”

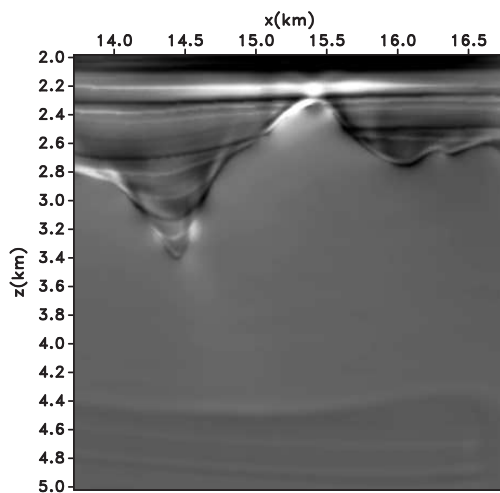


Figure 4: New imaging condition I_2 in the “case study”

ADAPTIVE REDUCTION OF IMAGING ARTIFACTS

The theory assumes sources and receivers distributed all over surface $\delta\mathbb{D}$ that bounds the imaging domain. In practice, the subsurface illumination is always limited and often has complicated and irregular patterns in complex models. In addition, the imaging condition (7) relies on unique and well-posed back-extrapolation of the scattered wavefields: this is seldom achievable in practice from pressure-only seismic data combined with inaccurate subsurface models. Consequently, the estimate of the scattered-wave power from the back-propagated receiver fields is also inaccurate. This, as we show here, calls for the image I_5 to be adaptively added to the classic image I_0 .

Just as crosscorrelation of scattered waves account for the cancellation of spurious arrivals in seismic interferometry (Fleury et al., 2010), we expect the autocorrelation of scattered wavefield G_S to play a similar role in the estimation of artifacts in nonlinear imaging. This makes it possible to consider applying adaptive filtering techniques. The signature of the artifacts observed in Figure 2 is comparable to the well-known RTM artifacts (Yoon and Marfurt, 2006). As suggested by Guitton et al. (2007), the suppression of such artifacts may benefit from the use of non-stationary filtering. Using the regularized non-stationary regression method implemented by Fomel (2009), the image I_5 provides a model for the artifacts in order to build a local matching filter, and removes the artifacts from the classic image I_1 . The filtered image I'_2 is the result of an adaptive imaging condition potentially suitable for nonlinear imaging. The reduction of the imaging artifacts can also be optimized by signal prediction filtering of I_1 by analogy with adaptive subtraction of multiples (Spitz, 1999; Guitton, 2005).

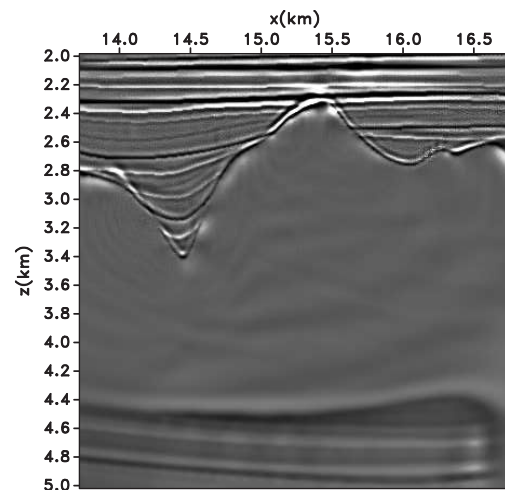


Figure 5: New image I'_2 in the “case study”

We apply the adaptive imaging condition to images I_1 and I_5 obtained in the “study case”. After removing the imaging artifacts, the filtered image I'_2 is shown in Figure 5. Comparing image I'_2 to image I_2 (Figure 4), the definition of the image structure is improved. Some low-frequency artifacts still visible in image I_2 have been attenuated.

Adaptive imaging condition for nonlinear imaging

ON THE CONNECTION WITH RTM IMAGING

The reasoning that leads toward the adaptive imaging condition relies on a parallel between representation theorems for scattered waves and imaging condition. In practice, only an estimate of the scattered wavefield is obtained by extrapolation. In RTM, the recorded data is back-propagated with a two-way propagator in a background velocity model. Only multiply-scattered waves that originate from the sharp boundary of this velocity model can be mapped properly in the image. Back-propagation also gives rise to discrepancies with the scattered wavefields such as backscattered waves that contribute to RTM artifacts. Finally, the limited aperture affects both the reconstruction of the receiver wavefield, and the imaging condition. While scattering representation theorems allow for an insightful descriptions of the nonlinear imaging problem, further work is still needed to clarify many different aspects that influence its practical performance.

The imaging condition (7) potentially accounts for the imaging artifacts due to multiply scattered waves that are extrapolated with the correct kinematics. RTM is applied to the synthetic data recorded at receivers located at 2 km depth, and modeled with the stratigraphic model (Figure 1(b)). Figure 6 and 7 present the classic image I_1 , and the image I_S obtained by autocorrelation of the receiver wavefield, respectively. After applying the adaptive imaging condition, the filtered image I'_2 is shown in Figure 8. Empirically, the image appears improved, and particularly, for the sediment layers on the top of salt body. However, while the imaging condition (7) in principle accounts for nonlinear scattering artifacts associated with the true scattered field G_S , the dominant contribution to RTM artifacts are associated with the backscattered waves that are estimated from the extrapolation of the receiver wavefield under severe experimental and model limitations. Further investigation into issues such as back-propagation, boundary conditions and aperture effects is necessary to extract more from the potential value of our method for extrapolated wavefields.

CONCLUSION

To image complex subsurface structures, nonlinear scattering cannot be neglected. Approaching this imaging problem with scattering theory leads to define a new adaptive imaging condition that can be potentially applied toward nonlinear imaging. The use of this method for RTM imaging reveals limitations that are subjects for ongoing research. Improving the understanding of the connection between imaging condition and representation theorems is crucial to achieve practical value of our imaging condition in enhancing nonlinear imaging practice.

ACKNOWLEDGEMENTS

Clement Fleury acknowledges the support of the sponsors of the Center for Wave Phenomena at Colorado School of Mines. We thank Roel Snieder (CSM) and Huub Douma for insightful discussions. We thank ION/GXT for supporting this research and for granting permission for publication.

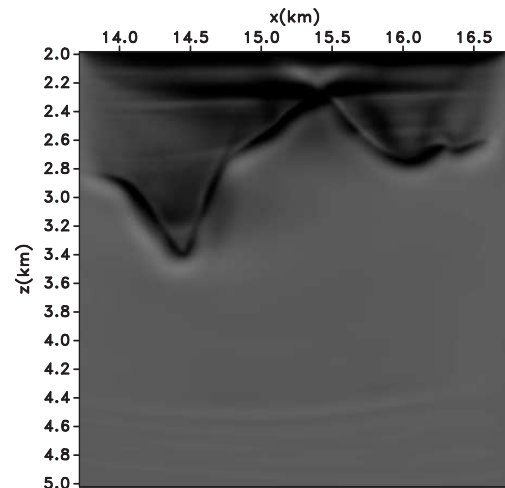


Figure 6: Classic image I_1 for RTM

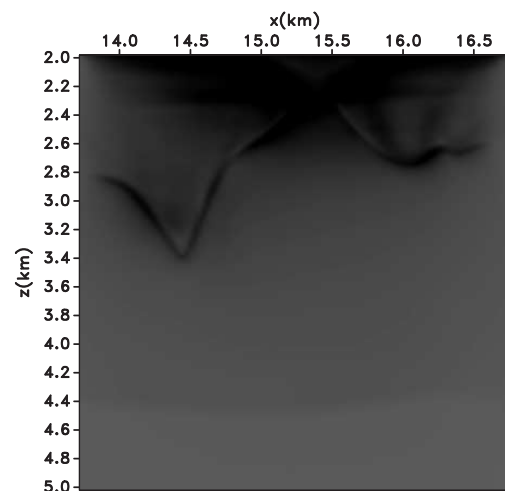


Figure 7: Image I_S for RTM

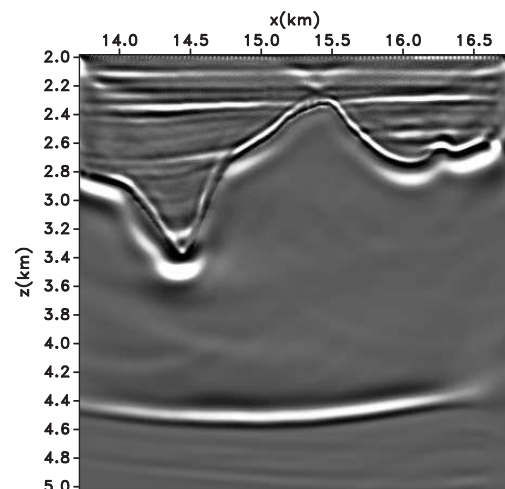


Figure 8: New image I'_2 for RTM

EDITED REFERENCES

Note: This reference list is a copy-edited version of the reference list submitted by the author. Reference lists for the 2010 SEG Technical Program Expanded Abstracts have been copy edited so that references provided with the online metadata for each paper will achieve a high degree of linking to cited sources that appear on the Web.

REFERENCES

- Baysal, E., D. Kosloff, and J. Sherwood, 1983, Reverse time migration: *Geophysics*, **48**, 1514–1524, [doi:10.1190/1.1441434](https://doi.org/10.1190/1.1441434).
- Carney, P., J. Schotland, and E. Wolf, 2004, Generalized optical theorem for reflection, transmission, and extinction of power for scalar fields: *Physical Review E: Statistical, Nonlinear, and Soft Matter Physics*, **70**, no. 3, 036611, [doi:10.1103/PhysRevE.70.036611](https://doi.org/10.1103/PhysRevE.70.036611).
- Claerbout, J., 1971, Toward a unified theory of reflector map-ping: *Geophysics*, **36**, 467, [doi:10.1190/1.1440185](https://doi.org/10.1190/1.1440185).
- , 1985, *Imaging the earth's interior*: Blackwell Scientific Publications, Inc.
- Esmersey, C., and M. Oristaglio, 1988, Reverse-time wave-field extrapolation, imaging, and inversion: *Geophysics*, **53**, 920, [doi:10.1190/1.1442529](https://doi.org/10.1190/1.1442529).
- Flury, C., R. Snieder, and K. Larner, 2010, General representation theorem for perturbed media and application to Green's function retrieval for scattering problems: Center for Wave Phenomena Annual report, CWP-671, CWP-662.
- Fomel S., 2009, Adaptive multiple subtraction using regularized nonstationary regression: *Geophysics*, **74**, no. 1, V25, [doi:10.1190/1.3043447](https://doi.org/10.1190/1.3043447).
- Guitton, A., 2005, Multiple attenuation in complex geology with a pattern-based approach: *Geophysics*, **70**, no. 4, V97, [doi:10.1190/1.1997369](https://doi.org/10.1190/1.1997369).
- Guitton, A., B. Kaelin, and B. Biondi, 2007, Least-squares attenuation of reverse-time-migration artifacts: *Geophysics*, **72**, no. 1, S19, [doi:10.1190/1.2399367](https://doi.org/10.1190/1.2399367).
- McMechan, G., 1983, Migration by extrapolation of time-dependent boundary values: *Geophysical Prospecting*, **31**, no. 3, 413–420, [doi:10.1111/j.1365-2478.1983.tb01060.x](https://doi.org/10.1111/j.1365-2478.1983.tb01060.x).
- Pratt, R., 1999, Seismic waveform inversion in the frequency domain, Part 1: Theory and verification in a physical scale model: *Geophysics*, **64**, 888–901, [doi:10.1190/1.1444597](https://doi.org/10.1190/1.1444597).
- Rickett, J., and P. Sava, 2002, Offset and angle-domain common image-point gathers for shot-profile migration: *Geophysics*, **67**, 883–889, [doi:10.1190/1.1484531](https://doi.org/10.1190/1.1484531).
- Sava, P., and S. Fomel, 2006, Time-shift imaging condition in seismic migration: *Geophysics*, **71**, no. 6, S209, [doi:10.1190/1.2338824](https://doi.org/10.1190/1.2338824).
- Sava, P., and I. Vasconcelos, 2010, Extended imaging condition for wave-equation migration: *Geophysical Prospecting*, no. [doi:10.1111/j.1365-2478.2010.00888.x](https://doi.org/10.1111/j.1365-2478.2010.00888.x).
- Snieder, R., K. van Wijk, M. Haney, and R. Calvert, 2008, Cancellation of spurious arrivals in Greens function extraction and the generalized optical theorem: *Physical Review E: Statistical, Nonlinear, and Soft Matter Physics*, **78**, no. 3, 036606, [doi:10.1103/PhysRevE.78.036606](https://doi.org/10.1103/PhysRevE.78.036606).
- Spitz, S., 1999, Pattern recognition, spatial predictability, and subtraction of multiple events: *The Leading Edge*, **18**, no. 1, 55, [doi:10.1190/1.1438154](https://doi.org/10.1190/1.1438154).

- Tarantola, A., 1984, Inversion of seismic reflection data in the acoustic approximation: *Geophysics*, **49**, 1259–1266, [doi:10.1190/1.1441754](https://doi.org/10.1190/1.1441754).
- Vasconcelos, I., P. Sava, and H. Douma, 2010, Wave-equation extended images via image-domain interferometry: *Geophysics*.
- Vasconcelos, I., R. Snieder, and H. Douma, 2009, Representation theorems and Greens function retrieval for scattering in acoustic media: *Physical Review E: Statistical, Nonlinear, and Soft Matter Physics*, **80**, no. 3, 036605, [doi:10.1103/PhysRevE.80.036605](https://doi.org/10.1103/PhysRevE.80.036605).
- Yoon, K., and K. Marfurt, 2006, Reverse-time migration using the Poynting vector: *Exploration Geophysics*, **37**, no. 1, 102–107, [doi:10.1071/EG06102](https://doi.org/10.1071/EG06102).